https://doi.org/10.1061/(ASCE)CC.1943-5614.0001106

BEHAVIOR OF LARGE-SCALE HYBRID FRP-CONCRETE-STEEL MULTITUBE CONCRETE COLUMNS UNDER AXIAL COMPRESSION

C. W. Chan[a]; T. Yu[b] and Y. L. Bai[c]

Abstract:

The combined use of an FRP tube with steel and concrete to form hybrid structural members has attracted increasing research attention. Hybrid FRP-concrete-steel multitube concrete columns (MTCCs) are a new form of such members, comprising an external FRP tube and a number of internal steel tubes, with all the space inside the tubes filled with concrete. Hybrid MTCCs allow the use of small-scale standard steel tube products to construct large-scale columns, and possess many advantages including excellent ductility, as demonstrated by recent studies. The existing studies on MTCCs, however, have been limited to the testing of small-scale specimens. For a new column form particularly suitable for large-scale construction, the potential size effect on the behavior of MTCCs needs to be clarified. This paper presents the first-ever experimental study on large-scale MTCCs through the testing of specimens with an outer diameter (for circular specimens) or side length (for square specimens) of 500 mm, and a height of 1500 mm. The configuration of steel tubes in these specimens, designed to be similar to real columns, are different from those in the small-scale MTCCs reported by the existing studies. The test results show that the large-scale MTCCs all possess excellent structural performance including ample ductility, and that the size effect appears to be negligible for MTCCs with sufficient confinement. The test results also show that the configuration of steel tubes may have a significant effect on the behavior of the confined concrete in MTCCs. In addition, an analytical method based on the transformed section approach and an existing model for FRP-confined concrete-filled steel tubes is presented and shown to provide close predictions of the test results in the present study.

Keywords: Large-scale columns; Hybrid columns; Tubular columns; Confinement; Fiber-reinforced polymer (FRP); Steel; Concrete.

[a]PhD Candidate, School of Civil, Mining and Environmental Engineering, Faculty of Engineering and Information Sciences, University of Wollongong, Wollongong, NSW 2522, Australia.

[b]Professor, Department of Civil and Environmental Engineering, The Hong Kong Polytechnic University, Hong Kong, China (corresponding author), E-mail address: tao-cee.yu@polyu.edu.hk.

[c]Associate Professor, Key Laboratory of Urban Security and Disaster Engineering of Ministry of Education, Beijing University of Technology, Beijing, China.

1 INTRODUCTION

In the last two decades, extensive studies have been conducted on the use of fiber-reinforced polymer (FRP) for new construction (Teng et al. 2007; Hollaway 2010). In particular, the combined use of an FRP tube with steel and concrete to form hybrid structural members has attracted increasing research attention (e.g. Teng et al. 2007; Karimi et al. 2011; Fanggi and Ozbakkaloglu 2015; Yu et al. 2019). In these hybrid members, the FRP tube typically serves as a corrosion-resistant skin and a confining device for the steel and concrete, while the steel serves as ductile longitudinal reinforcement for the concrete to resist axial load and bending moments. Various forms of steel reinforcement have been used in such applications, including steel bars (e.g., Yu and Teng 2010), steel plates (Yu et al. 2017a), a steel tube (e.g., Teng et al. 2007, 2018; Fanggi and Ozbakkaloglu 2015) and a steel section (e.g., Karimi et al. 2011; Huang et al. 2017), leading to various forms of FRP-concrete-steel hybrid tubular structural members (Yu 2018).

FRP-concrete-steel hybrid multitube concrete columns (MTCCs) are a new form of hybrid structural members recently proposed by the second author (Yu et al. 2017b). An MTCC comprises an external FRP tube and a number of internal steel tubes, with all the space inside the tubes filled with concrete [e.g., Figs. 1(a) and 1(e)]. In MTCCs, the three materials (i.e., FRP, concrete and steel) are optimally combined to achieve several advantages, including their excellent ductility, excellent durability and ease for construction (Yu et al. 2017b). In particular, the new column form allows the use of small-scale (SS) standard steel tube products to construct large-scale columns, thereby eliminating the difficulties associated with the manufacturing, transportation, and installation of large steel tubes. Compared with concrete-filled FRP tubes (CFFTs) with steel bars, the use of steel tubes allows a relatively large steel volume ratio to be used without affecting the quality of concrete casting. Consequently, the stiffness and load capacity of MTCCs can be larger compared with steel bar-reinforced CFFTs of the same dimensions. In addition, the circular internal steel tubes provide effective confinement to the concrete in MTCCs, leading to further enhanced load capacities and ductility. Furthermore, the use of steel tubes eliminates the need for or significantly reduces the amount of transverse reinforcement (e.g., steel stirrups) and facilitates the construction process.

Yu et al. (2017b) present the conceptual development of MTCCs as well as the results from a series of axial compression tests on SS circular MTCC specimens to demonstrate some of their expected advantages. Chan et al. (2018) present an experimental study on the axial compressive behavior of square MTCCs by testing SS specimens. The results from Yu et al. (2017b) and Chan et al. (2018) confirmed that the concrete in both circular and square MTCCs is very well confined, and the buckling of internal steel tubes is effectively prevented, leading to very ductile structural responses. The experimental studies presented in Yu et al. (2017b) and Chan et al. (2018), however, have been limited to SS specimens with the outer diameter/side length being less than or about 200 mm.

Many researchers (e.g., Carey and Harries 2005; Wang and Wu 2011; De Luca et al. 2010; Ozbakkaloglu 2013; Wang et al. 2016; Zeng et al. 2018) have investigated the size effects of FRP-confined concrete columns. In these studies, the effects of column size have been examined mainly in terms of: (1) the unconfined strength of concrete; and (2) the confinement effectiveness of FRP. The size effect on the unconfined strength of concrete in FRP-confined columns appears to be dependent on the shape of columns. For circular columns, the majority of the existing studies (e.g., Carey and Harries 2005; Ozbakkaloglu 2013) show that such size effect is insignificant, while some researchers (e.g., Wang and Wu 2011) observed that the unconfined strength of concrete decreased significantly with the column size. For square columns, the existing studies (e.g., De Luca et al. 2010; Wang et al. 2016; Zeng et al. 2018) generally agree that the size effect on the unconfined concrete strength cannot be ignored, but different studies proposed different reduction factors for it, which range at least from 0.78 to 0.94. If the size effect on the unconfined strength is properly considered, the existing studies (e.g., De Luca et al. 2010; Ozbakkaloglu 2013) generally show that the same stress-strain models of FRP-confined concrete can be directly used for specimens of various scales, as long as the concrete is sufficiently confined with a bilinear ascending stress-strain curve. This observation implies that for sufficiently-confined concrete in columns with the same confinement stiffness ratio: (1) the size effect on the slope of the second linear branch of the stress-strain curve can generally be ignored; and (2) the size effect on the ultimate axial strain at the rupture of FRP can generally be ignored if the same type of FRP is used.

As a variation of FRP-confined concrete columns, the behavior of MTCCs is complicated by the multiple steel tubes which provide significant additional confinement to the concrete. As a result, the conclusions obtained from tests of normal FRP-confined concrete columns on the size effects may not directly apply here. For example, it may be reasonable to expect that the size effect on the unconfined strength of concrete in square MTCCs is not as pronounced as in normal FRP-confined square columns because of the existence of multiple circular steel tubes in the former. Therefore, it is necessary to test large-scale (LS) MTCC specimens to clarify the size effects so that the results from SS specimens can be confidently used to develop design approaches. For a new column form particularly proposed for large-scale construction, the testing of LS specimens are also important to fully demonstrate the structural concept of MTCCs: the configurations of typical practical MTCCs [Figs. 1(a) and (e)] are difficult to be investigated through SS specimens whose size limits the number of steel tubes that can fit in (Yu et al. 2017b).

Against the above background, this paper presents the first-ever experimental study on LS-MTCCs. The LS specimens tested in the present study had an outer diameter (for circular specimens) or side length (for square specimens) of 500 mm, and a height of 1500 mm. The experimental program and results of the study are presented and discussed in the following sections.

2 EXPERIMENTAL PROGRAM

2.1 Test specimens

A total of 11 LS specimens were prepared and tested under concentric axial compression, including eight LS-MTCCs and three LS plain concrete-filled FRP tubes (LS-CFFTs) for comparison. Fig. 1 shows the cross-sections of the specimens while Table 1 summarizes their details. In Table 1, t_{frp} is the thickness of FRP tube; t_{st} and D are the thickness and diameter of steel tube, respectively; h is the height of specimens; and ρ_{st} is the steel volume ratio. The LS-MTCC specimens included five square and three circular specimens. The fibers in the FRP tube of all specimens were oriented at ±87° to the longitudinal direction.

The square specimens covered two thicknesses of FRP tube (i.e., 3.0 mm and 6.0 mm) and three steel tube configurations, which were formed by 16, 8 and 4 steel tubes, respectively [Figs. 1(a)-(c)]. The two FRP tube thicknesses were selected based on existing studies on FRP-confined concrete (Lam and Teng 2003b; Wang and Wu 2008), so that for CFFTs, the larger one (6.0 mm) leads to an approximately bilinear ascending axial load-strain curve (i.e. sufficiently-confined concrete) while the smaller one leads to an axial load-strain curve with a descending branch (i.e. weakly-confined concrete). The number of steel tubes was chosen to be a multiple of four (i.e. 16, 8 or 4) so that these tubes can be symmetrically placed inside a square FRP tube. The circular columns all had the same FRP tube with a thickness of 2.5 mm, and covered two steel tube configurations formed by 12 and 6 steel tubes, respectively [Figs. 1(e) and(f)]. For ease of comparison, three types of steel tubes (Types A-C) were selected for use in the LS-MTCC specimens so that the total volume ratio of steel (ρ_{st}) is similar (i.e., 4.23%-4.68%) for all the specimens despite their quite different configurations (see Table 1).

The selected volume ratios of steel in the present study are similar to those of typical FRP-concrete-steel hybrid tubular structural members in existing studies (e.g., Fanggi and Ozbakkaloglu 2015; Huang et al. 2017) and are generally higher than those of typical steel-reinforced concrete columns.

The three LS-CFFT specimens covered the three types of FRP tubes (i.e., two square ones and one circular one) used in the LS-MTCC specimens. All the LS specimens had a height of 1500 mm. The FRP tube of all the square specimens had an inner side length of 500 mm, while that of all the circular specimens had an inner diameter of 500 mm, leading to a height-to-diameter/side length ratio of 3:1. Similar height-to-diameter/side length ratios have been widely adopted in the existing experimental studies on the compressive behaviour of FRP-confined concrete columns (e.g., Fanggi and Ozbakkaloglu 2015; Teng et al. 2018; Huang et al. 2017; Zeng et al. 2018).

Each specimen is given a name for ease of reference. The name includes the following parts in sequence: (1) a letter ‘M’ or ‘F’ to represent MTCC and CFFT, respectively; (2) another letter ‘S’ or ’C’ to represent square and circular specimens, respectively; (3) a number followed by a letter ‘A’, ‘B’ or ‘C’ to represent the number and the type of inner steel tubes; (4) a two-digit number to represent the thickness of FRP tube. To ensure the repeatability of the results, two nominally identical specimens were prepared for each of two selected section configurations. For these specimens, their names end with an additional Roman numeral (“I” or “II”) to differentiate the two nominally identical specimens. For example, Specimen M-S-8B-3.0-I is the first square MTCC specimen with eight Type-B steel tubes and a 3.0 mm thick FRP tube.

2.2 Material properties

All specimens were cast in a single batch using ready-mix concrete with a maximum aggregate size of 10 mm. Two groups of three standard cylinders (150 mm x 300 mm) were tested at the beginning and the end of the LS specimen tests to determine the unconfined concrete strength during the test period (about three weeks), in accordance with AS1012.9 (2014). The average compressive strengths (f'_{co}) at the beginning and the end of the tests were found to be 34.4 MPa and 36.2 MPa, respectively. As the difference in the two strengths is relatively small, an average value of 35.3 MPa is used in the discussions in this paper. Due to an equipment issue, the axial strain corresponding to the peak stress of unconfined concrete (ε_{co}) was not measured in the tests, and a value of 0.228% is used in the discussions in this paper. This value was obtained using the unconfined concrete strength and the following equation proposed by Popovics (1973):

$$\varepsilon_{co} = 9.37 \times 10^{-4} \sqrt[4]{f'_{co}} \qquad (f'_{co} \text{ in MPa}) \qquad (1)$$

For each type of steel tubes, five steel coupons were cut in the longitudinal direction of the tube and were tested under tension in accordance with BS18 (1987). Three of the five steel coupons were cut away from the welding seam of the tube, while the other two included the welding seam to examine that effect. The key test results are summarized in Table 2, including the elastic modulus (E_{st}), yield stress (σ_y) and ultimate tensile stress (σ_u). The results show that the welding process led to significant increases in the yield stress and ultimate stress and slight decreases in the elastic modulus of the steel. In addition to the steel coupon tests, axial compression tests were conducted on three bare steel tubes of each type. The tested steel tubes all had a height-to-diameter ratio of 3:1 to eliminate the effects of end restraints and slenderness. The dimensions of these steel tubes and their average ultimate axial loads (L_{st}) obtained from the tests are also summarized in Table 2.

Three types of prefabricated glass FRP tubes were used in the present study, including (1) circular tube with an inner diameter of 500 mm and a nominal thickness of 2.5 mm, (2) square tube with an inner side length of 500 mm and a nominal thickness of 3 mm, and (3) square tube with an inner side length of 500 mm and a nominal thickness of 6 mm. All the FRP tubes were manufactured via a filament-winding process. The tubes all had a nominal fiber volume fraction of 49%, according to the data provided by the manufacturer. To obtain the mechanical properties of FRP tube, five FRP coupons were cut from a flat side of a 3 mm square FRP tube along its transverse direction, and were tested under tension in accordance with ASTM D3039/D3039M (2014). The test results showed that the FRP tubes had an average elastic modulus of 33.3 GPa and an average tensile strength of 573 MPa in the transverse direction, based on a nominal thickness of 3 mm and an average rupture strain of 0.0172. Despite the large size of the FRP tubes, the circular tube used in the present study had a weight of only 9.67 kg.

2.3 Preparation of specimens

The preparation of LS-MTCC specimens included the following procedures: (1) putting the steel tubes in place to form a “steel wall” with a temporary holder; (2) employing point electric arc welding near the ends of the steel tubes to secure them in the desired configuration before removing the temporary holder; (3) welding four steel rods to each end of the steel wall as spacers to ensure that they were concentrically placed in the FRP tube; (4) attaching strain gauges at the mid-height of the steel tubes; (5) putting the FRP tubes in place; (6) casting concrete; (7) strengthening the two ends of each specimen using carbon fiber sheets of 100 mm width. The preparation of LS-CFFT specimens is similar, except that Steps (1)-(4) were not needed. For practical applications of MTCCs, the placement of steel tubes may also be facilitated by adopting steel angle brackets or steel bars (Yu et al. 2017).

2.4 Test set-up and instrumentation

A total of six linear variable displacement transducers (LVDTs) were employed for each specimen, including two LVDTs (i.e., LVDT-A and B) to measure the axial shortening of the specimen and four LVDTs to measure the axial deformation of the 500 mm mid-height region. The layout of the LVDTs is shown in Fig. 2(a).

For each square LS-MTCC specimen, a total of 16 lateral strain gauges were attached to the inner steel tubes and the outer FRP tube. For each circular LS-MTCC specimen, a total of 14 lateral strain gauges were attached to the inner steel tubes and the outer FRP tube. In addition, six axial strain gauges (i.e., four on the outer FRP tube and two on the inner steel tubes) were attached to each LS-MTCC specimen. The layout of the strain gauges is shown in Fig. 2(b). The layout of strain gauges on the FRP tube of the CFFT specimens is the same as that for the corresponding MTCC specimens.

All compression tests on the LS specimens were conducted using a 7200-tonne Popwil (Hangzhou, PRC) compression test machine at the Beijing University of Technology (Fig. 3), with a displacement control rate of 0.6 mm/min. The compressive load was applied to the entire cross-section of the specimens. To ensure uniform loading to the specimen ends, the two end surfaces were ground before test. A preload of 1000 kN was applied for each LS specimen to check the instrumentation; this load is only about 1/8-1/12 of the nominal squash load of the specimen and thus had no effect on the compressive behavior of the specimen. The nominal squash load is calculated by $N_0 = A_{st}\,\sigma_y + A_c\,f'_{co}$, where A_{st} and A_c are the cross-sectional areas of steel and concrete, respectively. The specimens were then unloaded to near zero force before the formal compression test. A data logger was employed to simultaneously record the test data, including strain gauge readings, loads from the test machine and displacements from the LVDTs.

In general, the failure of FRP-confined concrete columns is controlled by the rupture of FRP under hoop tension. Such failure is normally accompanied with release of a large amount of energy. Therefore, the failure of LS FRP-confined specimens such as those tested in the present study might be risky for the testing machine and the surroundings. Due to safety concerns, the compression tests of all the LS-MTCC specimens were intentionally terminated when the average hoop strain of FRP reached about 50% of the FRP rupture strain obtained from tensile coupon tests, as per the strict requirement of the laboratory. While the use of this measure means that the ultimate state of the specimens could not be captured in the tests, it still allows the main characteristics of the column behavior (e.g., with a sufficiently long second branch of the axial load-axial strain curves) to be examined, as further discussed in the following sections. Similar to the observation of previous tests on LS FRP-confined specimens (e.g., Wang and Wu 2011; Zeng et al. 2018), the failure modes of LS-MTCCs are expected to be similar to those of SS specimens and readers may refer to Yu et al. (2017b) and Chan et al. (2018) for such details.

3.0 RESULTS AND DISCUSSIONS

3.1 Axial load-strain behavior

The axial load-strain curves of all the LS specimens are shown in Fig. 4, where the axial strains were obtained from the average readings of the four LVDTs covering the 500 mm mid-height region (Fig. 2). In this paper, the axial strains were all obtained in this way unless otherwise specified. For the circular specimens, the curves are terminated at a point corresponding to the average FRP hoop strain of 0.008. For all the square MTCC specimens, the last point of the curves corresponds to the average FRP lateral strain of 0.008 at the corners. The curve of Specimen F-S-3.0 has a descending branch and it is terminated at an axial load which is equal to 80% of the peak load. Hereafter in this paper, the axial load and axial strain of the last point of the curves are referred to as the final axial load and final axial strain, respectively.

For all the MTCC specimens, the curves feature an approximately bilinear shape with two ascending branches (Fig. 4), which is similar to the results of other FRP-confined concrete columns with sufficient confinement (e.g., Lam and Teng 2003a; Yu et al. 2019). As expected, the curves of the MTCC specimens are significantly higher than that of the corresponding CFFT specimens because of the existence of internal steel tubes. Fig. 4(a) further shows that the slopes of the second branches of the curves of circular MTCC specimens are similar to and slightly larger than that of the corresponding circular CFFT specimen, while the final axial strains of the former are significantly larger than that of the latter. This observation confirms that the internal steel tubes in circular MTCC specimens play a significant role in providing additional confinement to the concrete.

For the square specimens with a 3.0 mm FRP tube, Fig. 4(b) shows that the curves of MTCC specimens are significantly different from that of the CFFT specimen (i.e., Specimen F-S-3.0). The MTCC specimens all have a continuously ascending curve while the curve of the CFFT specimen has a descending branch, suggesting that the effect of additional confinement from the internal steel tubes is particularly important when the FRP confinement is relatively weak. For the square specimens with a 6.0 mm FRP tube, the observation is similar to that of circular specimens: the MTCC specimen has a much longer curve than that of the CFFT specimen while the slopes of the second branches of the two are almost the same [Fig. 4(b)]. During the tests, a number of horizontal cracks appeared on the FRP tubes after the axial strain reached about 0.003 (Fig. 5). These cracks, due mainly to the axial straining of FRP, did not affect the general behavior of the specimens, as evident from the axial load-strain curves in Fig. 4. However, they may be considered as early warning signs in practical applications and should generally be avoided by design for the serviceability limit state.

The key test results of all specimens are summarized in Table 3. For consistency, all values in this table are rounded to three significant digits. In this table, $N_{exp,f}$ is the final axial load of the LS specimens; $\varepsilon_{c,f}$ is the final axial strain from the tests; $\varepsilon_{lfs,f}$ and $\varepsilon_{lc,f}$ are the final lateral strains of square specimens at the flat sides and the corners, respectively; $\varepsilon_{h,f}$ is the final hoop strain of circular specimens; N_0 is the nominal squash load and is calculated by $N_0 = A_{st}\,\sigma_y + A_c\,f'_{co}$, where A_{st} and A_c are the cross-section area of the steel tubes and the concrete, respectively, while f_y and f'_{co} are the yield stress of steel and unconfined strength of concrete, respectively. In this paper, the lateral strains of square LS specimens at the flat sides and the corners (i.e., $\varepsilon_{lfs,f}$ and $\varepsilon_{lc,f}$) were each averaged from four lateral strain gauges; while the hoop strain of circular LS specimens was averaged from eight hoop strain gauges.

It should be noted that although $N_{exp,f}$ is already significantly higher than N_0 (by up to around 30%), it does not represent the load capacity of the columns as the tests were terminated before the final failure. However, it can be observed that: (1) the test MTCCs generally have an approximately bilinear axial load-axial strain curves (Fig. 4); and (2) the lateral strain of the MTCCs generally increases linearly with the axial strain after a certain axial strain (Fig. 6). Therefore, based on the slope of the second linear branch of the axial load-axial strain curves and the lateral strain-axial strain curves, the ultimate load of the test MTCCs corresponding to the FRP rupture strain (i.e. 0.0172) may be estimated. Compared with $N_{exp,f}$, the so-estimated ultimate load is around 30% higher for the circular MTCCs, around 20% higher for the square MTCC with a 6.0 mm FRP tube, and around 10% higher for the square MTCCs with a 3.0 mm FRP tube except Specimen M-S-16A-3.0.

3.2 Effect of configuration of internal steel tubes

The LS-MTCC specimens tested in the present study all had a similar volume ratio of steel (see Table 1), so their results can be compared to directly illustrate the effect of configuration of steel tubes. It is evident from Fig. 4(a) that the axial load-strain curves of the three circular MTCC specimens are quite close to each other, suggesting that the variation of steel tube configuration (from 6-tube configuration to 12-tube configuration) in the present study has little effect on circular MTCCs.

By contrast, Fig. 4(b) shows that the steel tube configuration can have a significant effect on the behavior of square MTCCs. For the specimens with a 3.0 mm FRP outer tube, the 4-tube configuration and the 8-tube configuration led to very similar axial load-strain curves, but the curve of the specimen with 16 steel tubes (i.e., Specimen M-S-16A-3.0) is significantly lower than the others, despite the fact that all specimens had a similar steel volume ratio. This is believed to be due to the relatively slender steel tubes (height-to-diameter ratio = 17.1) used in Specimen M-S-16A-3.0, whose tendency to globally buckle is higher than the tubes in other specimens. When tested under compression, such slender steel tubes in an MTCC may have slightly bent outwards especially when the confinement from the external FRP tube is relatively weak, as was the case for Specimen M-S-16A-3.0. It is believed that the outward bending of the steel tubes led to reduced lateral confinement to the concrete core and thus a lower axial load-strain curve.

To further illustrate this issue, the lateral-axial strain curves of all the square LS-MTCC specimens with a 3.0 mm FRP tube are compared in Fig. 6, where the lateral strain was averaged from readings of the eight lateral strain gauges (i.e., four at flat sides and four at corners). Unlike other specimens in the figure, the lateral strains of Specimen M-S-16A-3.0 in the early stage increased rapidly, while the slope of the lateral-axial strain curve (i.e., the dilation rate) became significantly lower than other specimens after axial strain of 0.005. This observation suggests that the FRP tube at the mid-height of Specimen M-S-16A-3.0 significantly expanded well before the peak load of the concrete was reached due to the early outward bending of the internal steel tube. As a result, the load of Specimen M-S-16A-3.0 remained nearly constant after the transition point of the axial load-strain curve [Fig. 4(a)], in contrast to the considerably increasing load for other LS-MTCC.

It should be noted that in practical applications, such outward bending of steel tubes in MTCCs should generally be prevented by properly selecting the height-to-diameter ratio of steel tubes, and/or increasing the confinement stiffness of FRP tube and the thickness of concrete cover. When necessary, additional steel stirrups may also be used outside the steel tubes to provide additional constraints.

3.3 Effect of thickness of FRP tube

The effect of thickness of FRP tube is obvious for the CFFT specimens, as shown in Fig. 4(b) and Table 3. Compared with Specimen F-S-3.0 with a 3.0 mm FRP tube, Specimen F-S-6.0 had much larger load capacity and ductility. In addition, the axial load-strain curve of the latter has an approximately bilinear ascending shape while that of the former has a descending branch due to the insufficient confinement.

By contrast, the effect of FRP thickness is not as pronounced for the MTCC specimens. Fig. 4(b) shows that the curves of Specimens M-S-8B-3.0-I, II (with a 3.0 mm FRP tube) are only slightly lower than that of Specimen M-S-8B-6.0 (with a 6.0 mm FRP tube), but the latter is much longer with a larger final axial strain. This observation suggests that the additional FRP thickness has only a small effect on the second-stage stiffness of the square MTCC specimens, but it may significantly affect the ductility of the specimens. This can be further explained by the lateral-axial strain curves of the three specimens (i.e., M-S-8B-3.0-I, II and M-S-8B-6.0), as shown in Figs. 6(a) and (b), where the lateral strains are averaged from the strain readings of flat sides and corners, respectively. It is evident that at the same axial strain, the lateral expansion of the specimen with a thicker tube (M-S-8B-6.0) is significantly lower than that of their counterparts with a thinner tube (M-S-8B-3.0-I, II) [Figs. 6(a) and (b)].

3.4 Lateral expansion behavior

The hoop/lateral strain distributions of typical specimens are shown in Fig. 7 using the radar charts. For each specimen, the hoop/lateral strain distributions for various axial strain levels are shown in a subfigure.

For the square CFFT specimens (i.e., F-S-3.0 and F-S-6.0), the lateral strain distributions feature an approximately square-shaped pattern, with the lateral strain gauge readings at the four flat sides (i.e., S1, S2, S3, S4) being significantly larger than that at the four corners (i.e., S12, S23, S34 and S41) [Figs. 8(a) and (b)]. This is consistent with the findings reported by the existing studies (e.g., De Paula and Da Silva 2002; Huang et al. 2017); the relatively large lateral strain readings at the flat sides are partially due to their outward bending as a result of the expansion of concrete. By contrast, the hoop strain distributions of the circular CFFT and MTCC specimens are relatively uniform due to the symmetric nature of the specimens [Figs. 7(c) and (d)].

The lateral strain distributions of the square MTCC specimens appear to be dependent on the configuration of internal steel tubes. For most of the specimens (e.g., M-S-8B-3.0-I; M-S-4C-3.0; M-S-8B-6.0), the pattern of lateral strain distributions is similar to the circular specimens, with the lateral strains at the flat sides being comparable to those at the corners [Figs. 7(e)-(g)]. This is due to the significant additional confinement from the multiple concrete-filled steel tubes in the MTCC specimens, which effectively constrained the expansion of the concrete towards the flat sides. By contrast, for Specimen M-S-16A-3.0, the lateral strains at the flat side are significantly larger than those at the corners, leading to an approximately square-shaped pattern of the distributions [Fig. 7(h)]. This is believed to at least partially due to the outward bending of the slender steel tubes in this specimen, as discussed in Section 3.1.

3.5 Stress-strain behavior of confined concrete

The normalized axial stress-normalized axial strain curves of the concrete in all the specimens are shown in Fig. 8, in which the axial stress and axial strain are normalized by the unconfined concrete strength and the corresponding axial strain, respectively. The axial stress was obtained by dividing the load carried by the concrete by its cross-section area. For the CFFT specimens, the load carried by the concrete is assumed to be equal to the load measured during the test. For the MTCC specimens, the load carried by the concrete is assumed to be equal to the difference between the load carried by the specimen and the load carried by the steel tubes at the same axial strain; the latter was obtained using the results of the steel tubes loaded alone under compression. The axial load taken by the FRP tube, which was small, is ignored. Again, the curves of the concrete in the MTCC specimens are terminated at an average hoop strain of 0.008 (for circular specimens) or an average lateral strain at the corners of 0.008 (for square specimens).

Fig. 8(a) shows the curves for the three CFFT specimens. The concrete in the circular specimen (F-C-2.5) and that in the square specimen with a thick FRP tube (F-S-6.0) have a bilinear ascending stress-strain curve, which is typical for concrete sufficiently confined by FRP (Lam and Teng 2003a). The normalized axial stress at the transition point of the curve, however, is significantly different for the two specimens: it is approximately equal to 1.0 for the circular specimen, while is approximately equal to 0.9 for the square specimen. For the square specimen with a thin FRP tube (F-S-3.0), the curve has a descending branch after the transition point due to the relatively weak FRP confinement, but the transition point is almost the same as that of the other square specimen (F-S-6.0). It has been well recognized that the first branch of the stress-strain curve of FRP-confined concrete is similar to that of unconfined concrete (Lam and Teng 2003a). Therefore, the above observation suggests that the unconfined strength of the concrete in the large circular CFFT specimen (F-C-2.5) was about the same as the unconfined strength of standard small cylinders, while for the large square CFFT specimens, the unconfined concrete strength was reduced by about 10%. This is consistent with the findings reported by some previous studies (e.g., De Luca et al. 2010; Ozbakkaloglu 2013).

Fig. 8(b) compares the curves of all the circular MTCC specimens with that of the corresponding CFFT specimen. All the curves of the MTCC specimens feature an approximately bilinear ascending shape, and the transition points of the two branches of the curves all have a normalized axial stress slightly larger than 1.0 [Fig. 8(b)]. It is also evident that the curves of the MTCC specimens are significantly higher than that of the CFFT specimen because of the additional confinement from the steel tubes.

Fig. 8(c) compares the curves of all the square MTCC specimens with those of the corresponding CFFT specimens. Except Specimen M-S-16A-3.0, all the MTCC specimens have an approximately bilinear ascending curve. Specimen M-S-16A-3.0 may have suffered from the outward bending of the slender internal steel tubes as discussed above, so the concrete was not as well confined as in the other specimens. Nevertheless, the normalized axial stress of the transition point is shown to be slightly higher than 1.0 for all the curves of the large MTCC specimens. This observation suggests that different from square CFFTs, the size effect on the unconfined concrete strength is insignificant for square MTCCs.

3.6 Comparison between LS-MTCCs and SS-MTCCs: Square specimens

To further investigate the size effect on the confinement effectiveness of square MTCCs, the test results of the present study are compared with those presented in Chan et al. (2018) on square SS-MTCC specimens. The details of the specimens in comparison are summarized in Table 4, in which E_{frp} is the elastic modulus of FRP. In the comparison, focuses are placed on the size effect on: (1) unconfined strength; and (2) the second-stage stiffness of MTCCs representing the confinement effectiveness. It should be noted that although the steel configuration and steel volume ratio of the specimens in Chan et al. (2018) are not the same as those in the present study, these two variables have been shown to have only a minor effect on the second-stage stiffness of MTCCs (Chan et al. 2018).

Fig. 9 shows the comparison for the normalized stress-strain curves, while the comparison for the normalized lateral-axial strain curves are shown in Fig. 10. In both figures, the curves of the SS-MTCC specimens are also terminated at an average lateral strain of 0.008 at the corners, for ease of comparison. It is evident from Fig. 9 that the curves of the LS-MTCC specimens are generally close to those of the SS-MTCC specimens, although considerable differences exist in the final axial strain of different specimens. These differences can be explained by Fig. 10, which shows evidently the different lateral expansion behavior of these specimens. Such differences in the lateral expansion behavior are not a surprise, as these specimens had quite different volume ratios of steel and different type of FRP tube (Table 4). It is easy to understand that the lateral expansion of concrete depends on the amount of confining materials (i.e., FRP and steel), so that the SS specimens, which had a larger steel volume ratio (see Table 4), generally had a longer curve than their LS counterparts. This observation is also consistent with the findings by Chan et al. (2018) through a comparison made among SS-MTCCs with different steel volume ratios.

Based on the above discussions, it is not unreasonable to conclude that (1) there is no evidence of any significant size effect on the confinement effectiveness of square MTCCs; (2) the volume ratios of steel and the confinement stiffness of the FRP tube, within the ranges of the respective values in Table 4, do not have a significant effect on the second-stage stiffness of the concrete in square MTCCs, but may have a considerable effect on its deformation capacity.

3.6 Comparison between LS-MTCCs and SS-MTCCs: Circular specimens

Similarly, the test results of the present study are compared with those presented in Yu et al. (2017b) on circular SS-MTCC specimens to investigate the size effect. The details of the specimens in comparison are summarized in Table 5.

Figs. 11 and 12 show the comparisons for the normalized stress-strain curves and the normalized lateral-axial strain curves, respectively, in which all the curves are terminated at an average hoop strain of 0.008. Figs. 11 and 12 show that the LS-MTCC specimens generally have higher normalized stress-strain curves but smaller final axial strains. These appear to be no evidence of size effect on the confinement effectiveness. The smaller final axial strains of LS-MTCC specimens are believed to at least partially due to their relatively smaller steel volume ratio (see Table 5), which led to a quicker lateral expansion of the specimens (Fig. 12). The higher second branches of these specimens may be due to the combined effects of the following factors: (1) the unconfined concrete strength of the LS specimen (35.3 MPa) is lower than that of the LS specimen (45.0 MPa); (2) at the same axial strain, the hoop strain of the LS specimens was higher, leading to a larger hoop stress in the FRP tube; (3) the different steel configurations in the LS and SS specimens; and/or (4) the scatter of test results.

3.7 Comparison with predictions of a simple analytical method

A simple analytical method was proposed for circular MTCCs based on Teng et al.'s (2013) model for FRP-confined concrete-filled steel tubes (F-CFSTs). In Teng et al.'s (2013) model, the axial stress-axial strain responses of concrete and steel are generated through an incremental and iterative procedure. For a given axial strain, the axial stress of concrete is determined using an active-confinement model (Jiang and Teng 2007) based on the confining pressure (σ_r), which can be calculated by the following equation considering the contributions from both the steel tube and FRP:

$$\sigma_r = \frac{2\,\sigma_{h,st} t_s + 2 E_{frp} t_{frp} \varepsilon_h}{D_c} \qquad (2)$$

where $\sigma_{h,st}$ is the hoop stress in the steel tube; E_{frp}, t_{frp} and ε_h are the elastic modulus, thickness and hoop strain of FRP, respectively; and D_c is the diameter of the concrete.

For a given axial strain (ε_c), the hoop strain of FRP (ε_h) can be calculated by the following equation using the confining pressure:

$$\frac{\varepsilon_c}{\varepsilon_{co}} = 0.85\left(1 + 8\frac{\sigma_r}{f'_{co}}\right)\left\{\left[1 + 0.75\left(\frac{\varepsilon_h}{\varepsilon_{co}}\right)\right]^{0.7} - exp\left[-7\left(\frac{\varepsilon_h}{\varepsilon_{co}}\right)\right]\right\} \qquad (3)$$

The steel tube is assumed to be an elastic-perfectly plastic material, and its axial strain and hoop strain are assumed to be the same as those of concrete considering strain compatibility. With the axial strain and hoop strain, the axial stress and hoop stress of steel tube can be determined based on the Hook's Law for the elastic range and based on the J_2 flow theory for the plastic range.

Once the axial stresses of concrete and steel tube are determined, the axial load taken by the column can be determined by:

$$N = \sigma_c A_c + \sigma_{c,st} A_{st} \qquad (4)$$

where σ_c and $\sigma_{c,st}$ are the axial stresses of concrete and steel, respectively. The reader may refer to Teng et al. (2013) for more details of the model.

In the simple analytical method, an MTCC is transformed into an equivalent F-CFST so that Teng et al.'s (2013) model can be used: the parameters of the external FRP tube remain unchanged, while the multiple internal steel tubes in MTCCs are transformed to an equivalent large steel tube which has an outer diameter being the same as the inner diameter of the external

FRP tube, and a cross-section area being the same as the sum of all the small steel tubes. The thickness of the equivalent large steel tube ($t_{st,eq}$) is given in Table 5.

In this way, the behavior of the concrete in an MTCC can be approximated by that in the equivalent F-CFST using Teng et al.'s (2013) model. The predictions of the analytical method are compared with the test results of typical LS and SS specimens in terms of both axial load-strain curves and hoop-axial strain curves (Figs. 14 and 15). In making the predictions, the final experimental hoop strain (i.e., 0.008) was adopted so that the predictions can compare with the test results in terms of the final axial strain and axial load.

It is evident from Fig. 14 that although the analytical method slightly overestimates the axial load-strain curves of some specimens, the predictions are generally in reasonable agreement with the test results. The slight overestimation may be due to the assumption adopted in the transformation method: in MTCCs part of the concrete is neither inside the steel tube nor surrounded by the steel tube, while in F-CFSTs the concrete is all subjected to combined confinement from the FRP and thee steel tube.

Fig. 15 shows that the analytical method can provide reasonably accurate predictions of the hoop-axial strain curves of both LS and SS specimens, suggesting that the lateral expansion behavior of MTCCs depend mainly on the FRP confinement stiffness and steel volume ratio but not the steel tube configuration.

4.0 CONCLUSIONS

This paper has presented results from an experimental study involving axial compression tests of LS-MTCCs with a square or circular FRP confining tube. The main test variables included the shape of cross-section, the configuration of internal steel tubes and the thickness of FRP tube. Based on the test observations, results and discussions presented in this paper, the following conclusions can be drawn:

1. The large-scale MTCCs all possessed excellent structural performance including ample ductility. The effectiveness of the confinement provided by the internal steel tubes is particularly pronounced when the FRP tube is relatively weak and/or when the column is of a non-circular shape (i.e. when the stress-strain curve of the concrete in the corresponding CFFT has a descending branch before FRP rupture).
2. The size effect on the unconfined concrete strength is significant for square CFFTs, but not for circular CFFTs.
3. The size effects on the behavior of MTCCs, in terms of the unconfined concrete strength, axial load-strain curve and lateral-to-axial strain curve, were not observed from the test results.
4. For MTCC specimens with very slender steel tubes, the confinement effectiveness may be negatively affected by the outward bending of the steel tubes due to their tendency of global buckling. The configuration of steel tubes may thus have a significant effect on the behavior of the confined concrete in MTCCs. In practical applications, such outward bending of steel tubes should generally be avoided by properly selecting the steel tubes, FRP tube and the concrete cover thickness, or by providing additional steel stirrups when necessary.
5. The volume ratio of steel may have a significant effect on the ultimate axial strain of MTCCs, but does not seem to significantly affect the second-stage stiffness of the columns.
6. The analytical method based on the transformed section approach and an existing model for FRP-confined concrete-filled steel tubes can provide reasonable predictions of the test results of the test specimens without outward bending of the steel tubes.

The present study has been limited to short columns in which the second order effect on the column behavior is negligible. Future research is needed to investigate the behavior of slender MTCCs. In slender MTCCs, the steel tubes may have a high tendency of global buckling, so a focus of future research should be on the development of a reliable design approach for preventing such global buckling of steel tubes. For a given confinement stiffness of FRP tube and concrete cover thickness, a limit of height-to-diameter ratio of steel tubes may be specified/calculated, beyond which additional steel stirrups should be provided.

ACKNOWLEDGEMENT

The authors are grateful for the financial support provided by the Australian Research Council (Project ID: DP170102992) and the National Natural Science Foundation of China (Project ID: 51778019). The authors also wish to thank Messrs Yufeng Zhang and Lihui Wang for their valuable contribution to the experimental work.

DATA AVAILABILITY STATEMENT

Some or all data, models, or code that support the findings of this study are available from the corresponding author upon reasonable request.

REFERENCES

AS1012.9 (2014). “Compressive strength tests- concrete, mortar and grout specimens”, *Method of Testing Concrete,* Standards Australia.

ASTM D3039/D3039M-17 (2017). *Standard test method for tensile properties of polymer matrix composite materials*, American Society for Testing and Materials.

BS18 (1987). *Method for tensile testing of metals (including aerospace materials)*, British Standards Institution.

Carey, S. A. and Harries, K. A. (2005). “Axial behavior and modeling of confined small-, medium-, and large-scale circular sections with carbon fiber-reinforced polymer jackets”, *ACI Structural Journal*, 102(4), 596.

Chan, C. W., Yu, T. and Zhang, S. S. (2018). “Compressive behaviour of square fibre-reinforced polymer–concrete–steel hybrid multi-tube concrete columns”, *Advances in Structural Engineering*, 21(8), 1162-1172.

De Luca, A., Nardone, F., Matta, F., Nanni, A., Lignola, G. P. and Prota, A. (2010). “Structural evaluation of full-scale FRP-confined reinforced concrete columns”, *Journal of Composites for Construction*, ASCE, 15(1), 112-123.

De Paula, R. F. and Da Silva, M. G. (2002). "Sharp edge effects on FRP confinement of RC square columns", *Proceedings, the 3rd International Conference on Composites in Infrastructure*, San Francisco, California.

Fanggi, B. A. L. and Ozbakkaloglu, T. (2015). "Square FRP–HSC–steel composite columns: Behavior under axial compression", *Engineering Structures*, 92, 156-171.

Hollaway, L. C. (2010). "A review of the present and future utilisation of FRP composites in the civil infrastructure with reference to their important in-service properties", *Construction and Building Materials*, 24(12), 2419-2445.

Huang, L., Yu, T., Zhang, S. S. and Wang, Z. Y. (2017). "FRP-confined concrete-encased cross-shaped steel columns: Concept and behaviour", *Engineering Structures*, 152, 348-358.

Jiang, T. and Teng, J. G. (2007). "Analysis-oriented stress-strain models for FRP–confined concrete", *Engineering Structures*, 29(11), 2968-2986.

Karimi, K., Tait, M. J. and El-Dakhakhni, W. W. (2011). "Testing and modeling of a novel FRP-encased steel–concrete composite column", *Composite Structures*, 93(5), 1463-1473.

Lam, L. and Teng, J. G. (2003a). "Design-oriented stress–strain model for FRP-confined concrete", *Construction and Building Materials*, 17(6-7), 471-489.

Lam, L. and Teng, J. G. (2003b). "Design-oriented Stress-Strain Model in rectangular columns." *Journal of Reinforced Plastics and Composites*, 22(13), 1149-1186.

Ozbakkaloglu, T. (2013). "Compressive behavior of concrete-filled FRP tube columns: Assessment of critical column parameters", *Engineering Structures*, 51, 188-199.

Popovics, S. (1973). "A numerical approach to the complete stress-strain curve of concrete", *Cement and concrete research,* 3(5), 583-599.

Teng, J. G., Hu, Y. M. and Yu, T. (2013). "Stress–strain model for concrete in FRP-confined steel tubular columns", *Engineering Structures*, 49, 156-167.

Teng, J. G., Yu, T., Wong, Y. L. and Dong, S. L. (2007). "Hybrid FRP–concrete–steel tubular columns: Concept and behavior", *Construction and Building Materials*, 21(4), 846-854.

Teng, J. G., Wang, Z., Yu, T., Zhao, Y. and Li, L. J. (2018). "Double-tube concrete columns with a high-strength internal steel tube: Concept and behaviour under axial compression", *Advances in Structural Engineering*, 21(10), 1585-1594.

Wang, D. Y., Wang, Z. Y., Smith, S. T. and Yu, T. (2016). "Size effect on axial stress-strain behavior of CFRP-confined square concrete columns", *Construction and Building Materials*, 118, 116-126.

Wang, L. M., and Wu, Y. F. (2008). "Effect of corner radius on the performance of CFRP-confined square concrete columns: Test." *Engineering Structures*, 30(2), 493–505.

Wang, Y. F. and Wu, H. L. (2011). "Size effect of concrete short columns confined with aramid FRP jackets", *Journal of Composites for Construction*, ASCE, 15(4), 535-544.

Yu, T. (2018). "Hybrid FRP-concrete-steel tubular members", *Proceedings, the* 9^{th} *International Conference on FRP Composites in Civil Engineering (CICE 2018)*, Paris, France, 17-19 July, 2018.

Yu, T. and Teng, J. G. (2010). "Design of concrete-filled FRP tubular columns: Provisions in the Chinese technical code for infrastructure application of FRP composites", *Journal of Composites for Construction*, ASCE, 15(3), 451-461.

Yu, T., Teh, L. H. and Hadi, M. N. (2017a). "High-strength steel plates in hybrid fiber-reinforced polymer–concrete–steel columns: Concept and behaviour", *Advances in Structural Engineering*, 20(5), 797-811.

Yu, T., Chan, C. W., Teh, L. and Teng, J. G. (2017b). "Hybrid FRP-Concrete-Steel Multi-Tube Concrete Columns: Concept and Behaviour", *Journal of Composites for Construction*, ASCE, 21(6), 04017044.

Yu, T., Zhao, H., Ren, T. and Remennikov, A. (2019). "Novel hybrid FRP tubular columns with large deformation capacity: Concept and behaviour", *Composite Structures*, 212, 500-512.

Zeng, J. J., Lin, G., Teng, J. G. and Li, L. J. (2018). "Behavior of large-scale FRP-confined rectangular RC columns under axial compression", *Engineering Structures*, 174, 629-645.

List of Tables

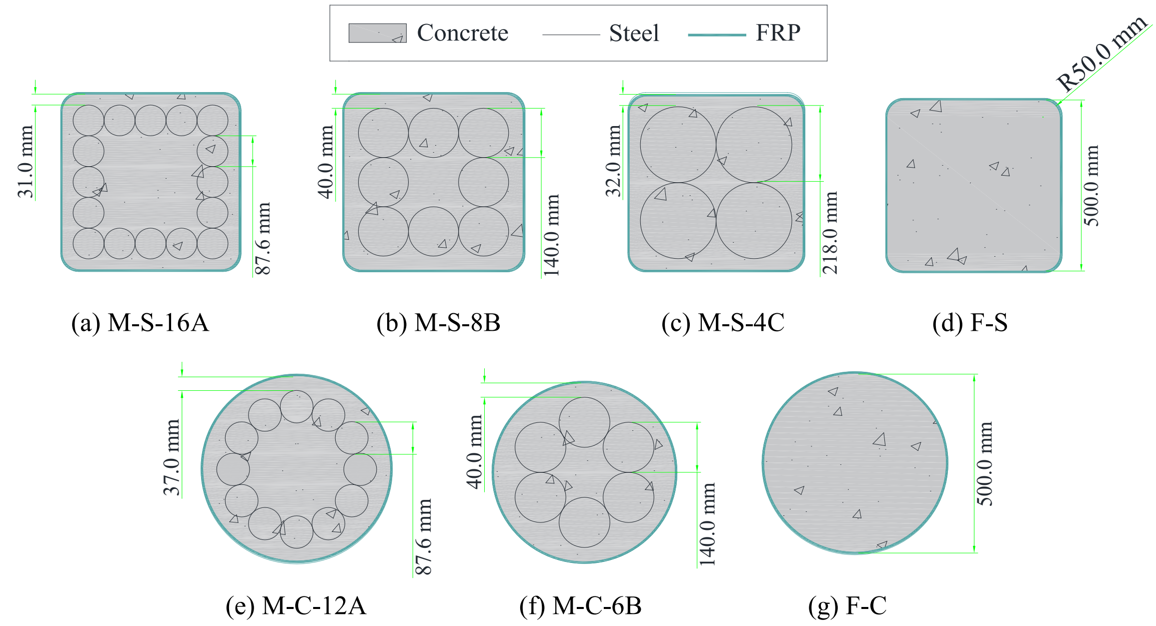

Fig. 1 Cross-sections of specimens

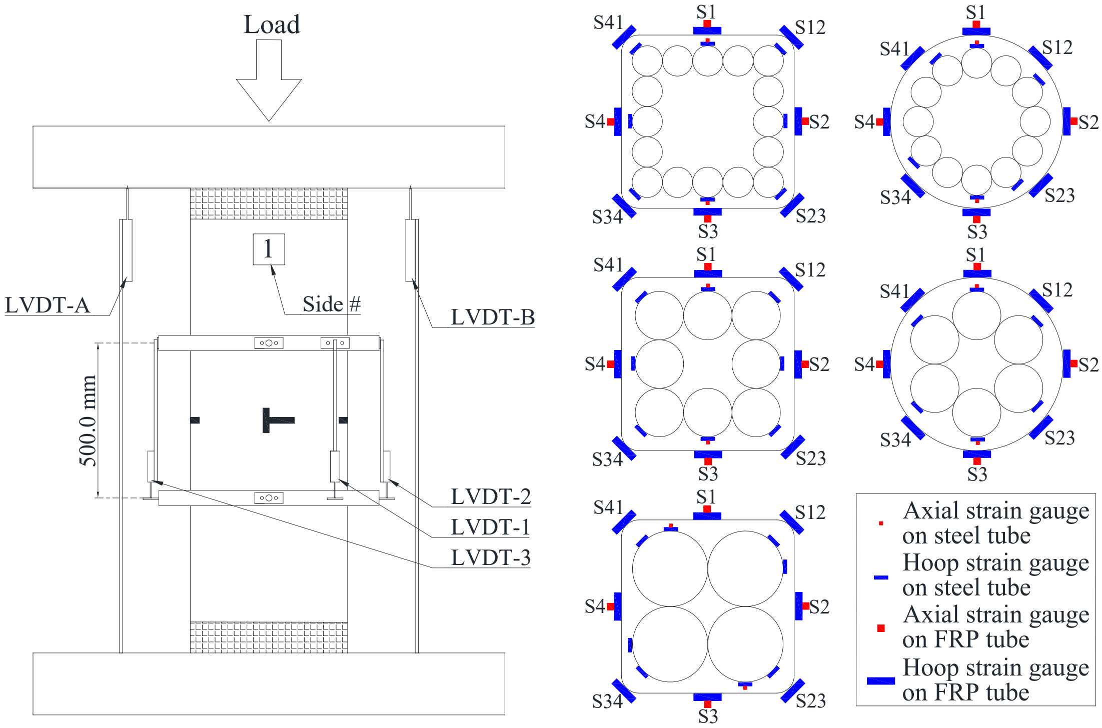

(a) Layout of LVDTs (b) Layout of strain gauges

Fig. 2 Test set-up

Fig. 3 Specimen during test

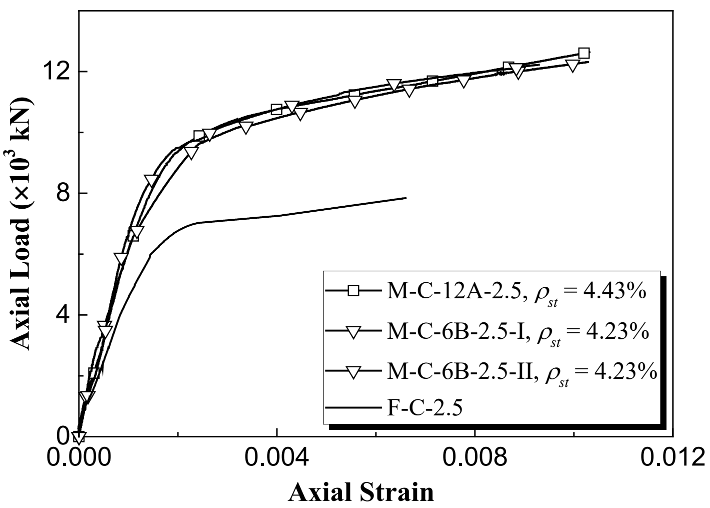

(a) Circular specimens

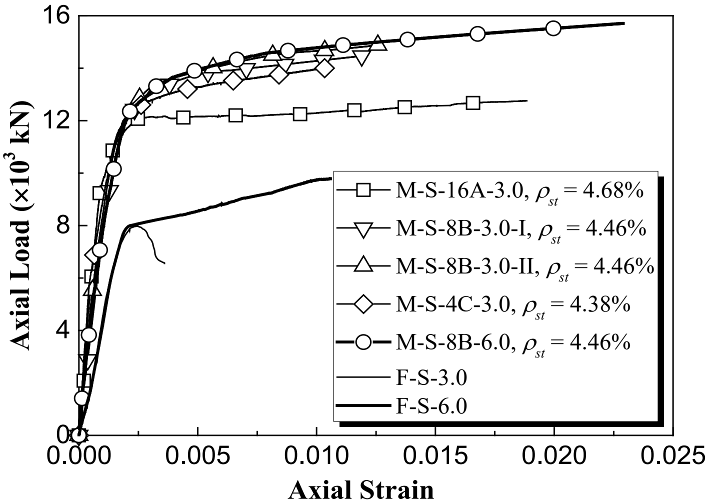

(b) Square specimens

Fig. 4 Axial load-axial strain curves

Fig. 5 Horizontal cracks on a typical specimen

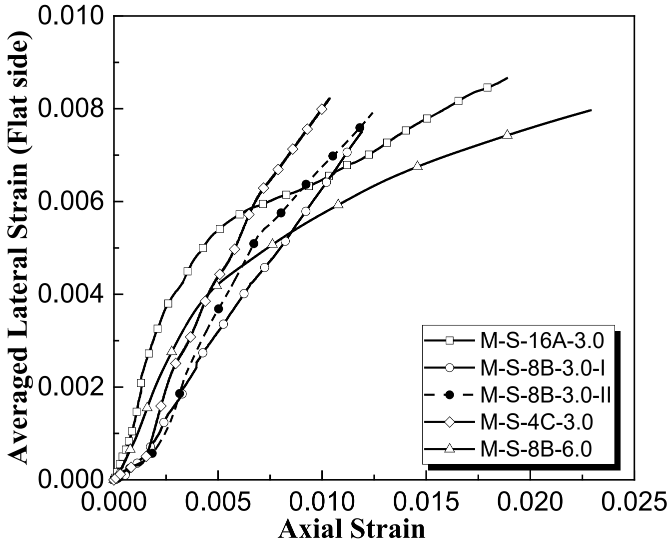

(a) Lateral strain from flat side

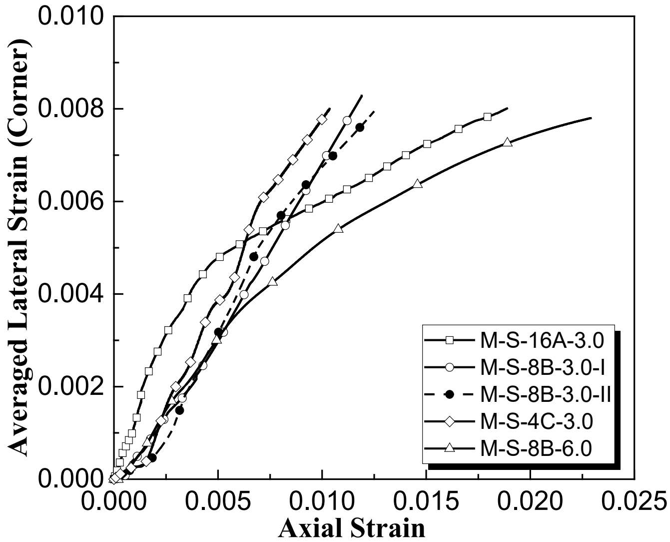

(b) Lateral strain from corner

Fig. 6 Lateral-axial strain curves of square MTCC specimens

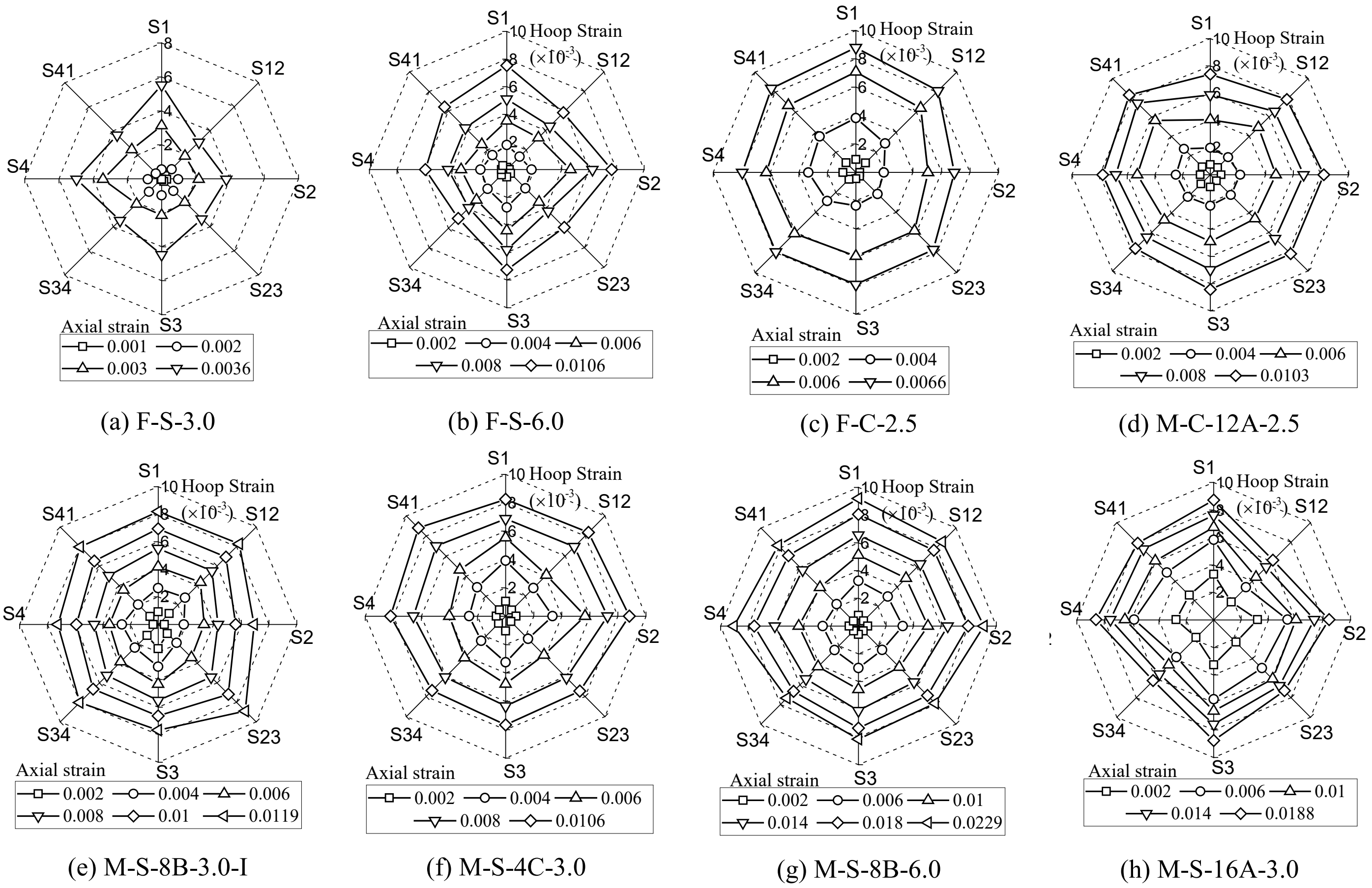

Fig. 7 Lateral strain distributions of typical specimens

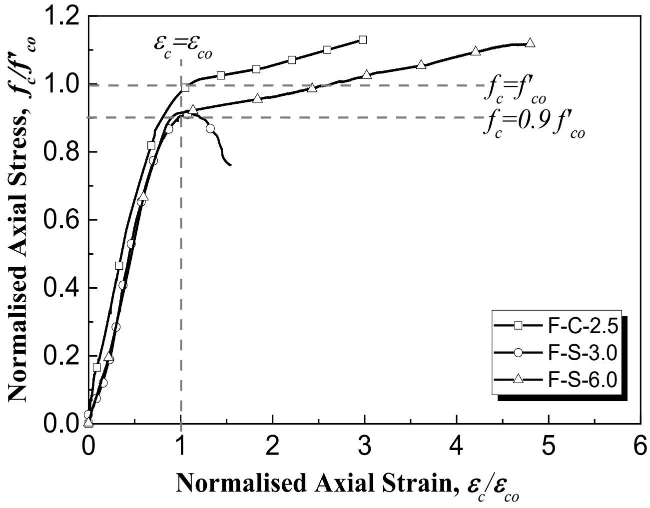

(a) CFFT specimens

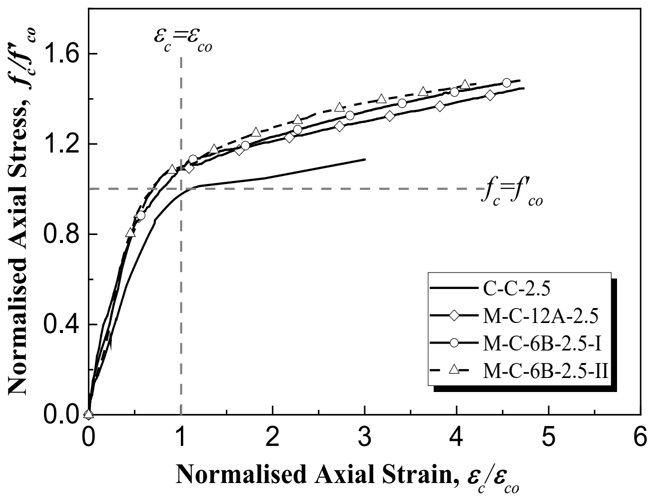

(b) Circular MTCC specimens

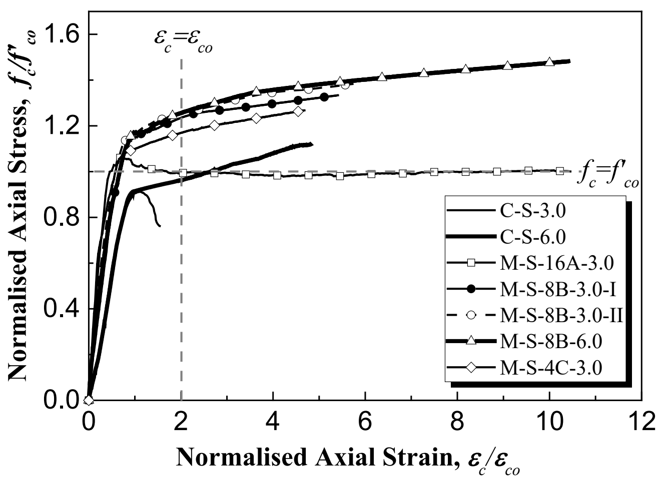

(c) Square MTCC specimens

Fig. 8 Normalised axial stress-normalised axial strain curves

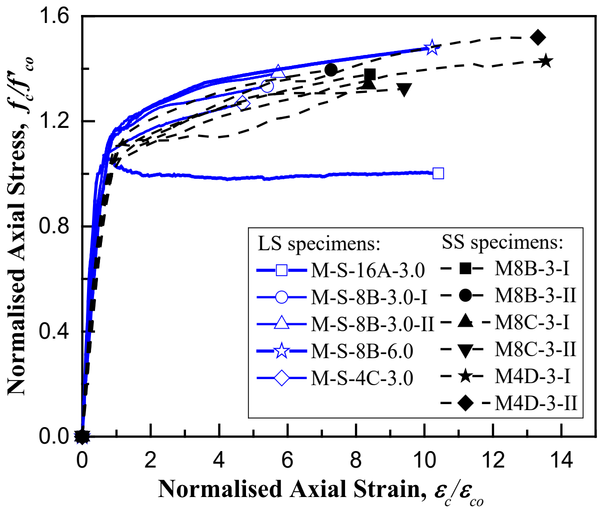

Fig. 9 Normalised axial stress-strain curves: Square MTCCs

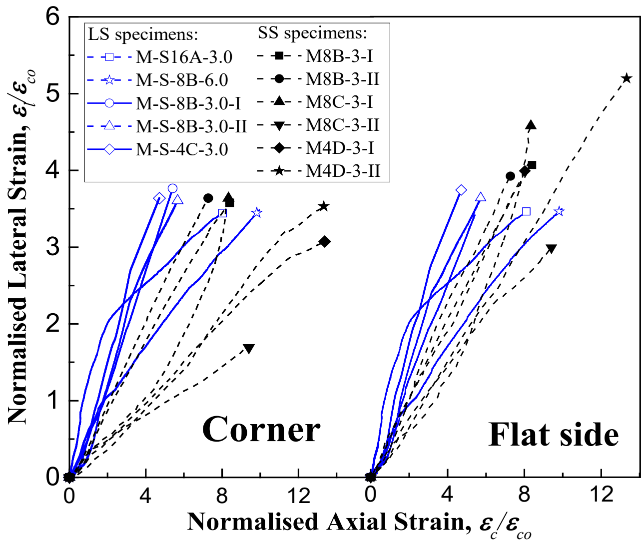

Fig. 10 Normalised lateral-axial strain curves: Square MTCCs

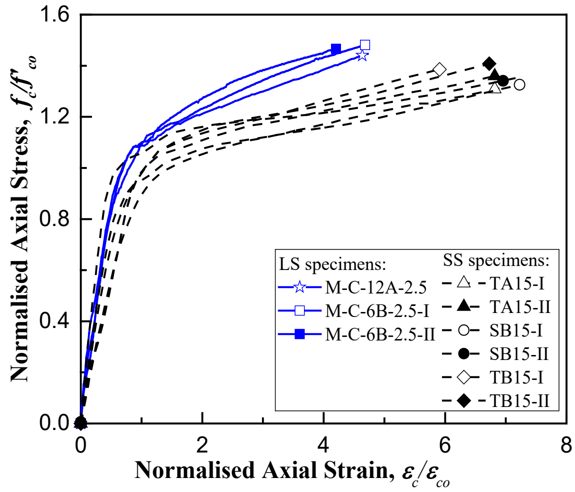

Fig. 11 Normalised stress-strain curves: Circular MTCCs

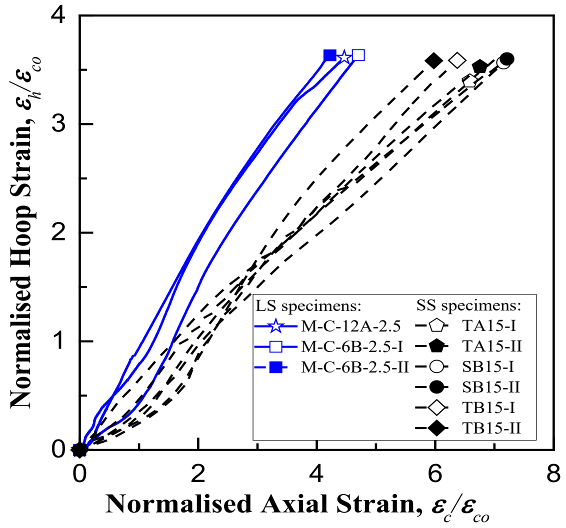

Fig. 12 Normalised lateral-axial strain curves: Circular MTCCs

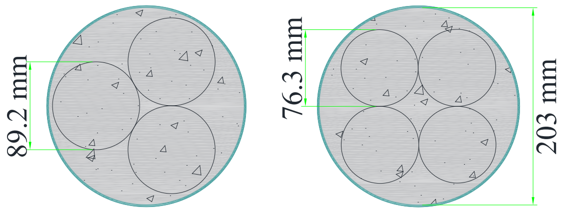

(a) Specimen TA15 (b) Specimen SB15

Fig. 13 Cross-section of SS-MTCCs

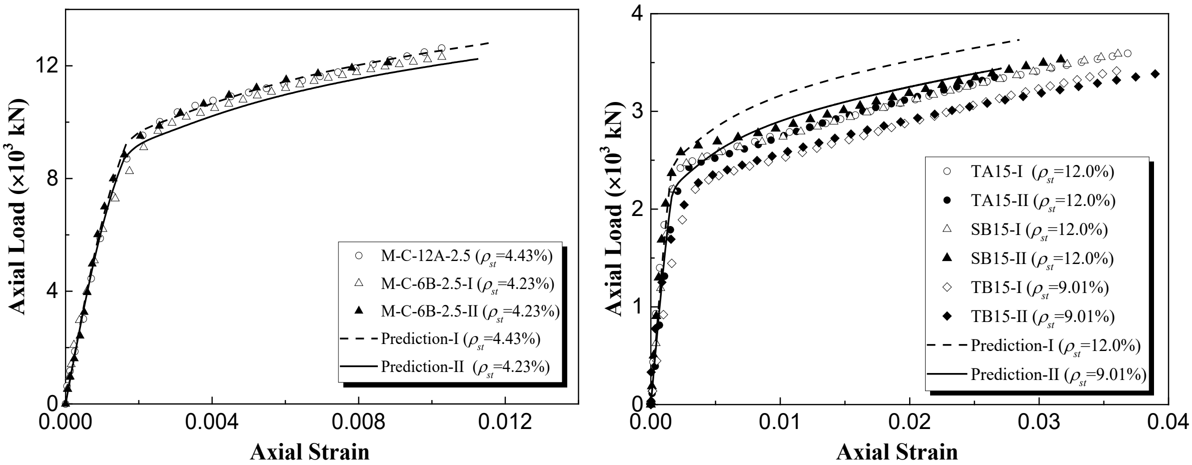

(a) LS-MTCCs (b) SS-MTCCs

Fig. 14 Performance of the analytical method: Axial load-axial strain curves

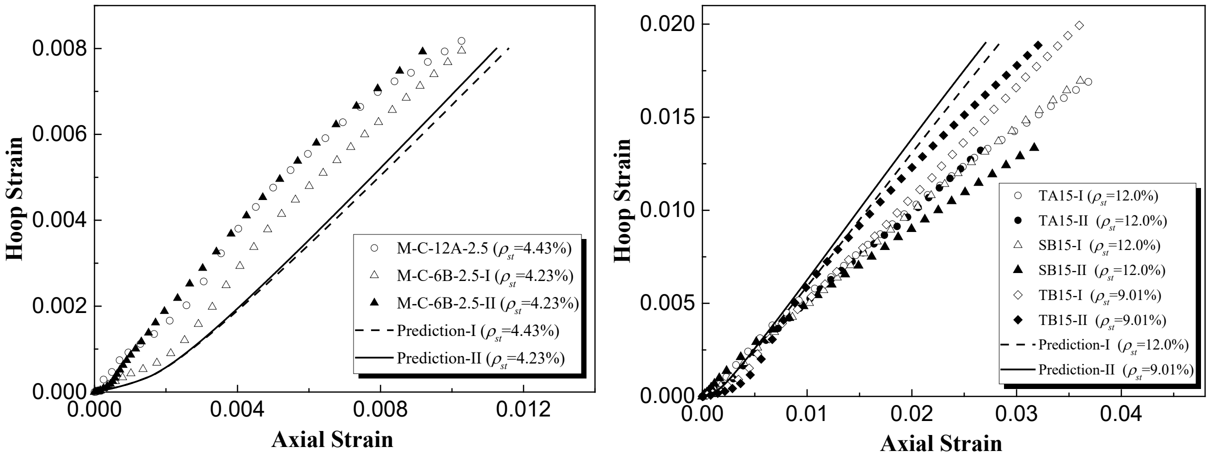

(a) LS-MTCCs (b) SS-MTCCs

Fig. 15 Performance of the analytical method: Hoop-axial strain curves